Serb. Astron. J. № 181 (2010), 19 - 29 **UDC 524.82–17**
DOI: 10.2298/SAJ1081019Z Original scientific paper

PRACTICAL STATISTICS FOR THE VOIDS BETWEEN GALAXIES

L. Zaninetti

Dipartimento di Fisica Generale, Via Pietro Giuria 1
10125 Torino, Italy

E–mail: *zaninett@ph.unito.it*

(Received: June 18, 2010; Accepted: September 17, 2010)

SUMMARY: The voids between galaxies are identified with the volumes of the Poisson Voronoi tessellation. Two new survival functions for the apparent radii of voids are derived. The sectional normalized area of the Poisson Voronoi tessellation is modelled by the Kiang function and by the exponential function. Two new survival functions with equivalent sectional radius are therefore derived; they represent an alternative to the survival function of voids between galaxies as given by the self-similar distribution. The spatial appearance of slices of the 2dF Galaxy Redshift Survey is simulated.

Key words. Methods: statistical – Cosmology: observations – large-scale structure of Universe

1. INTRODUCTION

The statistical analysis of the voids between galaxies is the topic of our research and the following catalogs have been explored: the two-degree Field Galaxy Redshift Survey (2dFGRS), see Patiri et al. (2006) and von Benda-Beckmann and Müller (2008), the Sloan Digital Sky Survey (SDSS), see Tikhonov (2007), and the combination of 2dFGRS and SDSS, see Tinker et al. (2008). The voids between galaxies are usually modelled by a survival function in the apparent radius as given by a modified exponential distribution, see Eq. (3) in von Benda-Beckmann and Müller (2008) or our Section 4; this fact is considered here a standard argument for comparison. The concept of Voronoi Diagrams dates back to the vortex theory applied to the solar system as developed in the 17th century; see Descartes (1644) and Fig. 1 in Aurenhammer and Klein (2000). The name is due to the two historical records by Voronoi (1907, 1908) and the applications to astrophysics beginning with Kiang (1966). The Voronoi diagrams represent a model of the voids between galaxies; see van de Weygaert and Icke (1989), Pierre (1990), Barrow and Coles (1990), Coles (1991), van de Weygaert (1991a), van de Weygaert (1991b), Zaninetti (1991), Ikeuchi and Turner (1991), Subba Rao and Szalay (1992), van de Weygaert (1994), Goldwirth et al. (1995), van de Weygaert (2002), van de Weygaert (2003), and Zaninetti (2006).

The Poisson Voronoi tessellation (PVT) is a particular case of the Voronoi tessellation in which the seeds are generated independently on the X, Y and Z axes in 3D through a subroutine which returns a random real number taken from a uniform distribution between 0 and 1. For practical purposes, the subroutine RAN2 was used; see Press et al. (1992).

On adopting an astrophysical point of view, the sectional PVT, $V_p(2,3)$, is very interesting because it allows a comparison with the voids as observed in slices of galaxies belonging to different catalogs such as the CFA2 catalog (Geller and Huchra 1989), the 2dfGRS (Norberg et al. 2002), the 6dF

Galaxy Survey (6dFGS) (Jones et al. 2004) or the SDSS (Einasto et al. 2003). The absence of: (i) a numerical analysis through the survival function of normalized areas in 2D and normalized volumes in 3D of PVT and (ii) a careful exploration of the statistical properties of $V_p(2,3)$, leads to the following questions:

(i) Is it possible to integrate the usual probability density functions (PDFs) which characterize the main parameters of 2D and 3D PVT in order to obtain an analytical expression for the survival function?
(ii) Is it possible to model the normalized areas of $V_p(2,3)$ with the known PDFs?
(iii) Can we transform the normalized volumes and areas into equivalent radius distributions?
(iv) Can we simulate the observed slices of galaxies as given, for example, by the 2dF Galaxy Redshift Survey?

In order to answer these questions, Section 2 reports the three major PDFs used to model the normalized area/volume of 2D/3D PVT as well as the results of the fit.

Section 3 reports the apparent distribution in effective radius of the 3D PVT as well as their associated survival functions.

Section 4 contains the self-similar survival function for voids between galaxies as well as the associated PDF.

Section 5 reports the fit of the normalized area distribution of the sectional PVT with the Kiang function and the exponential distribution.

Section 6 reports our actual knowledge of the photometric properties of galaxies as well as a Voronoi simulation.

It is important to point out that the PVT is not used as a technique to identify voids in existing data catalogs; see Ebeling and Wiedenmann (1993), Bernardeau and van de Weygaert (1996), Schaap and van de Weygaert (2000), Marinoni et al. (2002), Melnyk et al. (2006), van de Weygaert and Schaap (2009) and Elyiv et al. (2009).

The PVT formalism is here used conversely: to generate mock catalogs which are later calibrated by observations. On adopting the point of view of the statistical distributions, it is important to underline that the survival function is here identified with the cumulative void size distribution function. We briefly recall that the cumulative void size distribution function relates the number of voids to their size, analogously to the halo mass function which relates the number of dark matter halos to their mass.

2. THE ADOPTED DISTRIBUTIONS OF THE PVT

A PDF is the first derivative of a distribution function (DF) $F(x)$ with respect to x. In the case where the PDF is known but the DF is unknown, the following integral:

$$F(x) = \int_0^x f(x)dx \tag{1}$$

is evaluated. As a consequence, the survival function (SF) is:

$$SF = 1 - F(x) \quad . \tag{2}$$

2.1. The Kiang function

The gamma variate $H(x;c)$, as given by Kiang (1966), is:

$$H(x;c) = \frac{c}{\Gamma(c)}(cx)^{c-1}\exp(-cx) \quad , \tag{3}$$

where $0 \leq x < \infty$, $c > 0$, and $\Gamma(c)$ is the gamma function with argument c. The Kiang PDF has the mean:

$$\mu = 1 \quad , \tag{4}$$

and variance:

$$\sigma^2 = \frac{1}{c} \quad . \tag{5}$$

In the case of a 1D PVT, $c = 2$ is an exact analytical result and conversely c is supposed to be 4 or 6 for 2D or 3D PVTs, respectively, Kiang (1966). The DF of the Kiang function, DF_K, is:

$$DF_K = 1 - \frac{\Gamma(c, cx)}{\Gamma(c)} \quad , \tag{6}$$

where the incomplete Gamma function, $\Gamma(a,z)$, is defined by:

$$\Gamma(a,z) = \int_z^\infty \mathrm{e}^{-t}t^{a-1}dt \quad . \tag{7}$$

The survival function S_K is:

$$S_K = \frac{\Gamma(c, cx)}{\Gamma(c)} \quad . \tag{8}$$

2.2. Generalized gamma

The generalized gamma PDF with three parameters a, b, c, see Hinde and Miles (1980), Ferenc and Néda (2007), and Tanemura (2003), is:

$$f(x;b,c,d) = c\frac{b^{a/c}}{\Gamma(a/c)}x^{a-1}\exp\left(-bx^c\right) \quad . \tag{9}$$

The generalized gamma has the mean:

$$\mu = \frac{b^{-\frac{1}{c}}\Gamma\left(\frac{1+a}{c}\right)}{\Gamma\left(\frac{a}{c}\right)} \quad , \tag{10}$$

and a variance:

$$\sigma^2 = \frac{b^{-\frac{2}{c}}\left(+\Gamma\left(\frac{2+a}{c}\right)\Gamma\left(\frac{a}{c}\right) - \left(\Gamma\left(\frac{1+a}{c}\right)\right)^2\right)}{\left(\Gamma\left(\frac{a}{c}\right)\right)^2} \quad . \tag{11}$$

The DF of the generalized gamma is:

$$DF_{GG} = 1 - \frac{\Gamma\left(\frac{a}{c}, bx^c\right)}{\Gamma\left(\frac{a}{c}\right)} \quad . \tag{12}$$

The SF of the generalized gamma is:

$$S_{GG} = \frac{\Gamma\left(\frac{a}{c}, bx^c\right)}{\Gamma\left(\frac{a}{c}\right)} \quad . \tag{13}$$

2.3. Ferenc–Neda function

A new PDF has been recently introduced, Ferenc and Néda (2007), in order to model the normalized area/volume in a 2D/3D PVT:

$$FN(x;d) = C \times x^{\frac{3d-1}{2}} \exp\left(-(3d+1)x/2\right) \quad , \tag{14}$$

where C is a constant:

$$C = \frac{\sqrt{2}\sqrt{3\,d+1}}{2\,2^{3/2\,d}\left(3\,d+1\right)^{-3/2\,d}\Gamma\left(3/2\,d+1/2\right)} \quad , \tag{15}$$

and $d(d = 1, 2, 3)$ is the dimension of the space under consideration. We will call this function the Ferenc–Neda PDF; it has the mean:

$$\mu = 1 \quad , \tag{16}$$

and variance:

$$\sigma^2 = \frac{2}{3d+1} \quad . \tag{17}$$

The DF of the Ferenc–Neda function when $d = 2$ is:

$$DF_{FN2} = -\frac{49}{15}\frac{\sqrt{2}\sqrt{7}x^{5/2}\mathrm{e}^{-7/2\,x}}{\sqrt{\pi}} - 7/3\,\frac{\sqrt{2}\sqrt{7}x^{3/2}\mathrm{e}^{-7/2\,x}}{\sqrt{\pi}} - \frac{\sqrt{2}\sqrt{7}\sqrt{x}\mathrm{e}^{-7/2\,x}}{\sqrt{\pi}} + \mathrm{erf}\left(1/2\,\sqrt{2}\sqrt{7}\sqrt{x}\right), \tag{18}$$

where the error function $\mathrm{erf}(x)$ is defined as:

$$\mathrm{erf}(x) = \int_0^x 2\,\frac{\mathrm{e}^{-t^2}}{\sqrt{\pi}}dt \; . \tag{19}$$

The SF of the Ferenc–Neda function when $d = 2$ is:

$$S_{FN2} = 1 + \frac{49}{15}\frac{\sqrt{2}\sqrt{7}x^{5/2}\mathrm{e}^{-7/2\,x}}{\sqrt{\pi}} + 7/3\,\frac{\sqrt{2}\sqrt{7}x^{3/2}\mathrm{e}^{-7/2\,x}}{\sqrt{\pi}} + \frac{\sqrt{2}\sqrt{7}\sqrt{x}\mathrm{e}^{-7/2\,x}}{\sqrt{\pi}} - \mathrm{erf}\left(1/2\,\sqrt{2}\sqrt{7}\sqrt{x}\right) . \tag{20}$$

The DF of the Ferenc–Neda function when $d = 3$ is:

$$DF_{FN3} = 1 - \mathrm{e}^{-5\,x} - 5\,\mathrm{e}^{-5\,x}x - \frac{25}{2}\,\mathrm{e}^{-5\,x}x^2 - \frac{125}{6}\,\mathrm{e}^{-5\,x}x^3 - \frac{625}{24}\,x^4\mathrm{e}^{-5\,x} \; . \tag{21}$$

The SF of the Ferenc–Neda function when $d = 3$ is

$$S_{FN3} = \mathrm{e}^{-5\,x} + 5\,\mathrm{e}^{-5\,x}x + \frac{25}{2}\,\mathrm{e}^{-5\,x}x^2 + \frac{125}{6}\,\mathrm{e}^{-5\,x}x^3 + \frac{625}{24}\,x^4\mathrm{e}^{-5\,x} \quad . \tag{22}$$

2.4. Numerical results

In what follows, we will model the PVT in which the seeds are computed through a random process. The χ^2 is computed according to the formula:

$$\chi^2 = \sum_{i=1}^{N} \frac{(T_i - O_i)^2}{T_i} \quad , \tag{23}$$

where N is the number of bins, T_i is the theoretical value and O_i is the experimental value. The first test of the PDFs presented in the previous section can be done by analysing the Voronoi cell normalized area-distribution in 2D, see Table 1.

Table 1. Values of χ^2 for the cell normalized area-distribution function in 2D. T_i are the theoretical frequencies and O_i are the sample frequencies. We have 25087 Poissonian seeds and 40 intervals in the histogram.

PDF	parameters	χ^2
H(x;c) (Eq. (3))	c=3.55	83.48
f(x;d) (Eq. (14))	d=2	71.83
G(x;a,b,c) (Eq. (9))	a=3.15 b=2.72 c=1.13	58.9

Table 2 reports the parameters of the PDF of the volume distribution in 3D.

Table 2. Values of χ^2 for cell normalized volume-distribution function in 3D. T_i are the theoretical frequencies and O_i are the sample frequencies. We have 21378 Poissonian seeds and 40 intervals in the histogram.

PDF	parameters	χ^2
H(x;c) (Eq. (3))	c=5.53	93.86
f(x;d) (Eq. (14))	d=3	134.15
G(x;a,b,c) (Eq. (9))	a=4.68 b=3.87 c=1.18	58.59

Fig. 1 reports an example of SF in 2D PVT (areas) and Fig. 2 an example of SF in 3D PVT (volumes).

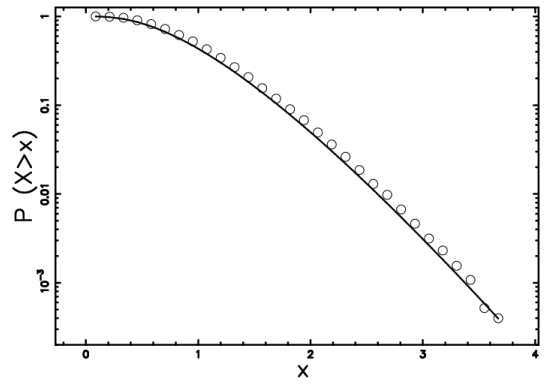

Fig. 1. *SF of normalized area-distribution function in 2D when we have 25087 Poissonian seeds and* 40 *intervals: the empty circles represent the Voronoi volumes and the full line the theoretical value of S_{GG} (generalized gamma function) as given by Eq. (13).*

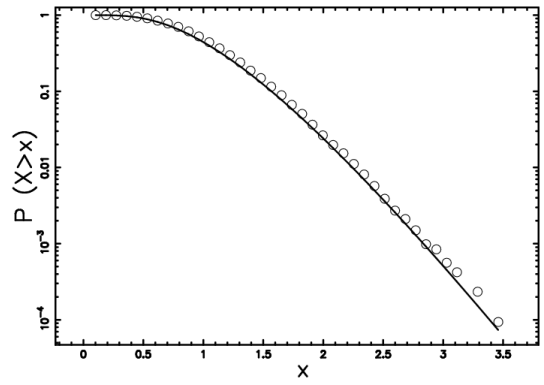

Fig. 2. *SF of normalized volume-distribution function in 3D when we have 21378 Poissonian seeds and* 40 *intervals: the empty circles represent the Voronoi volumes and the full line the theoretical value of S_K (Kiang function) as given by Eq. (8).*

3. RADIUS DISTRIBUTION OF THE 3D PVT

We now analyse the distribution in effective radius R of the 3D PVT. We assume that the volume of each cell, v, is:

$$v = \frac{4}{3}\pi(\frac{R}{\rho})^3 \quad , \tag{24}$$

where ρ is the length that connects the normalized radius to the observed one. In what follows, we derive the PDF for radius and related quantities for the Kiang function and Ferenc–Neda function.

3.1. Kiang function of the radius

The PDF, $H_R(R;c)$, of the radius corresponding to the Kiang function as represented by Eq. (3) is

$$H_R(R;c) = \frac{4\,c\left(4/3\,\frac{c\pi\,R^3}{\rho^3}\right)^{c-1} e^{-4/3\,\frac{c\pi\,R^3}{\rho^3}}\pi\,R^2}{\Gamma\,(c)\,\rho^3} \quad , \tag{25}$$

where $0 \leq R < \infty$, $c > 0$ and $\rho > 0$. The Kiang PDF of the radius has the mean:

$$\mu = 1/2\,\frac{\sqrt[3]{2}\sqrt[3]{3}\Gamma\,(1/3+c)}{\sqrt[3]{c}\sqrt[3]{\pi}\Gamma\,(c)}\rho \quad , \tag{26}$$

and variance:

$$\sigma^2 = \frac{1}{4}\frac{3^{\frac{2}{3}}2^{\frac{2}{3}}\left(\Gamma\,(2/3+c)\,\Gamma\,(c) - (\Gamma\,(1/3+c))^2\right)}{c^{2/3}\pi^{2/3}\,(\Gamma\,(c))^2}\rho^2 \tag{27}$$

The DF of the Kiang function of the radius is:

$$DF_{KR} = 1 - \frac{\Gamma\left(c, 4/3\,c\pi\,(\frac{R}{\rho})^3\right)}{\Gamma\,(c)} \quad . \tag{28}$$

The survival function of the radius is:

$$S_{KR} = \frac{\Gamma\left(c, 4/3\,c\pi\,(\frac{R}{\rho})^3\right)}{\Gamma\,(c)} \quad . \tag{29}$$

3.2. Ferenc–Neda function of the radius

The PDF as a function of the radius, obtained from Eq. (14) and inserting $d = 3$, is:

$$FN_R(R;d) = \frac{400000\,\pi^5 R^{14} e^{-\frac{20}{3}\,\frac{\pi\,R^3}{\rho^3}}}{243\,\rho^{15}} \quad . \tag{30}$$

The mean of the Ferenc–Neda function is:

$$\mu = 0.6\rho \quad , \tag{31}$$

and the variance is:

$$\sigma^2 = 0.0085\rho^2 \quad . \tag{32}$$

The DF of the Ferenc–Neda function of the radius when $d = 3$ is:

$$\begin{aligned} DF_{FN3R} = {} & \\ & 1 - e^{-\frac{20}{3}\,\frac{\pi\,R^3}{\rho^3}} - \frac{20}{3}\,e^{-\frac{20}{3}\,\frac{\pi\,R^3}{\rho^3}} R^3\pi\rho^{-3} \\ & -\frac{200}{9}\,e^{-\frac{20}{3}\,\frac{\pi\,R^3}{\rho^3}} R^6\pi^2\rho^{-6} \\ & -\frac{4000}{81}\,e^{-\frac{20}{3}\,\frac{\pi\,R^3}{\rho^3}} R^9\pi^3\rho^{-9} \\ & -\frac{20000}{243}\,e^{-\frac{20}{3}\,\frac{\pi\,R^3}{\rho^3}} R^{12}\pi^4\rho^{-12} \quad . \end{aligned} \tag{33}$$

The SF of the Ferenc–Neda function of the radius when $d = 3$ is:

$$S_{FN3R} = e^{-\frac{20}{3}\frac{\pi R^3}{\rho^3}} + \frac{20}{3} e^{-\frac{20}{3}\frac{\pi R^3}{\rho^3}} R^3\pi\rho^{-3} + \frac{200}{9} e^{-\frac{20}{3}\frac{\pi R^3}{\rho^3}} R^6\pi^2\rho^{-6} + \frac{4000}{81} e^{-\frac{20}{3}\frac{\pi R^3}{\rho^3}} R^9\pi^3\rho^{-9} + \frac{20000}{243} e^{-\frac{20}{3}\frac{\pi R^3}{\rho^3}} R^{12}\pi^4\rho^{-12} \quad . \tag{34}$$

4. SELF-SIMILAR VOID DISTRIBUTION

The statistics of the voids between galaxies have been analysed in von Benda-Beckmann and Müller (2008) with the following self-similar SF in the following, S_{SS}

$$S_{SS} = \mathrm{e}^{-\left(\frac{R}{s_1\lambda}\right)^{p_1} - \left(\frac{R}{s_2\lambda}\right)^{p_2}} \quad , \tag{35}$$

where λ is the mean separation between galaxies, s_1 and s_2 are length factors, and p_1 and p_2 are powers. The DF of the self-similar distribution is:

$$DF_{SS} = 1 - \mathrm{e}^{-\left(\frac{R}{s_1\lambda}\right)^{p_1} - \left(\frac{R}{s_2\lambda}\right)^{p_2}} \quad . \tag{36}$$

The PDF of the self-similar distribution is:

$$p_{SS}(R) = \frac{\mathrm{e}^{-(\frac{R}{s_1\lambda})^{p_1} - (\frac{R}{s_2\lambda})^{p_2}} ((\frac{R}{s_1\lambda})^{p_1} p_1 + (\frac{R}{s_2\lambda})^{p_2} p_2)}{R} . \tag{37}$$

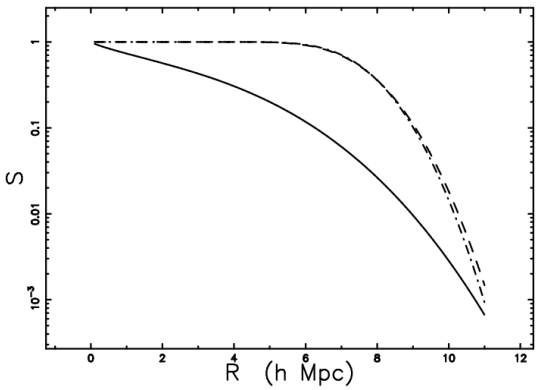

Fig. 3. *The survival function S_{SS} of the self-similar distribution in radius of $N/S1$ as represented by Eq. (35) (full line), the survival function, S_{FN3R}, for the Ferenc–Neda function of the radius as represented by Eq. (34) when $d = 3$, $\rho = 12.5$ Mpc and $\chi^2 = 4319$ with 100 points (dashed line). The survival function S_{KR} of the radius of the Kiang function as represented by Eq. (29) when $\rho = 12.5$ Mpc, $c = 5.53$ and $\chi^2 = 4076$ with 100 points (dot-dashed line).*

At present, it is not possible to find an analytical expression for the integral that defines the average value of the self-similar distribution.

A comparison of the survival function of self-similar voids with the survival function of the radii of the two PDFs analysed here is reported in Fig. 3.

The two fits of Fig. 3 are not satisfactory because we are making a comparison between the radius of projected voids and the 3D radii of the normalized volume distribution of the PVT. This fact is confirmed from the high values of χ^2 computed according to Eq. (23).

5. THE SECTIONAL PVT

The existence of voids between galaxies is normally deduced from a projected distribution in astronomical slices such as the 2dFGRS S3; see Fig. 1 in von Benda-Beckmann and Müller (2008). This fact motivates the analysis of the sectional Voronoi tessellation, also known as $V_p(2,3)$; see Okabe et al. (1992). A previous analysis has shown that a cell belonging to the intersection between an arbitrary plane and the faces of the Voronoi polyhedrons is almost surely a non-Voronoi cell; see details in Chiu et al. (1996). Here, we first model the normalized area-distribution $V_p(2,3)$ with Kiang PDFs as represented by Eq. (3), see Table 3.

Table 3. Values of χ^2 for the cell normalized area-distribution function of $V_p(2,3)$; here T_i are the theoretical frequencies and O_i are the sample frequencies. We have 8517 Poissonian seeds and 40 intervals in the histogram.

PDF	parameters	χ^2
H(x;c) (Eq. (3))	c=2.07	114.41
p(x;b) (Eq. (38))	d=1	85.38

In the case of n cuts, we can compute the average value of c, $\overline{c}$, and the standard deviation σ, see Table 4.

Table 4. Average value of c according to the Kiang function, Eq. (3)), for $V_p(2,3)$, when 50 cuts are considered. Here we have 25087 Poissonian seeds.

PDF	name	$\overline{c}$	σ
H(x;c) (Eq. (3))	Kiang	2.25	0.11

A test of this value can be performed on the unpublished manuscript of Ken Brakke available at http://www.susqu.edu/brakke/aux/downloads/papers/3d.pdf .

Table 4 of this paper is dedicated to the 3D plane cross-sectional statistics E(area) = 0.6858 and Var(area) = 0.2269. When a typical run of ours is normalized to the average value rather than to 1, our result is Var(area) = 0.2266 which means that our numerical evaluation differs by 2/10000 from the theoretical result. We recall that in the case of the normalized area-distribution function in 2D, we have

$c \approx 4$ and we can therefore speak of a decrease of c by a factor 2. The decrease of c for $V_p(2,3)$ was first derived in Fig. 4 of Zaninetti (2006).

Another PDF that can be considered in order to model the normalized area distribution of $V_p(2,3)$ is the exponential distribution:

$$p(x) = \frac{1}{b} \exp -\frac{x}{b} \quad , \tag{38}$$

which has the average value:

$$\overline{x} = b \quad . \tag{39}$$

In the case of the normalized areas, $b = 1$. Table 3 reports the χ^2 values of the two distributions adopted here. Once the statistics of the normalized area distribution of an arbitrary cut $V_p(2,3)$ are known, we can model the radius distribution. We therefore convert the area of each cell A to an equivalent radius R:

$$R = \sqrt{\frac{A}{\pi}} \quad . \tag{40}$$

We also briefly recall that the problem of stereology is to deduce the true size distribution $N(R)$ of 3D-volumes from the distribution $n(r)$ of apparent circles in 2D.

5.1. Kiang distribution of $V_p(2,3)$ in radius

The PDF, $H_{R23}(R;c)$, as a function of the radius corresponding to the Kiang function as represented by Eq. (3) for $V_p(2,3)$ is:

$$H_{R23}(R;c) = \frac{2\,c \left(\frac{c\pi\,R^2}{\rho^2}\right)^{c-1} \mathrm{e}^{-\frac{c\pi\,R^2}{\rho^2}} \pi\,R}{\Gamma(c)\,\rho^2} \quad , \tag{41}$$

where $0 \leq R < \infty$, $c > 0$ and $\rho > 0$. The Kiang PDF of the radius for $V_p(2,3)$ has the mean:

$$\mu = \frac{\rho\,\Gamma(c+1/2)}{\sqrt{c}\sqrt{\pi}\Gamma(c)} \quad , \tag{42}$$

and variance:

$$\sigma^2 = \frac{\rho^2 \left(c\,(\Gamma(c))^2 - (\Gamma(c+1/2))^2\right)}{c\pi\,(\Gamma(c))^2} \quad . \tag{43}$$

The DF of the Kiang function of the radius, DF_{KR23}, for $V_p(2,3)$ is:

$$DF_{KR23} = 1 - \frac{\Gamma\left(c, 2\,\frac{c\pi\,R^2}{\rho^2}\right)}{\Gamma(c)} \quad . \tag{44}$$

The survival function S_{KR23} of the radius for $V_p(2,3)$ is:

$$S_{KR23} = \frac{\Gamma\left(c, 2\,\frac{c\pi\,R^2}{\rho^2}\right)}{\Gamma(c)} \quad . \tag{45}$$

A comparison of the survival function of self-similar voids with the survival function of the radius for $V_p(2,3)$ of the exponential distribution is reported in Fig. 4.

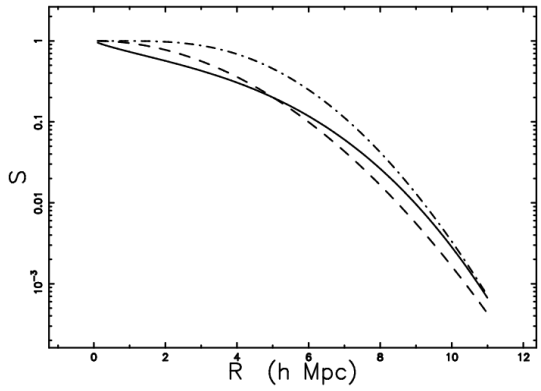

Fig. 4. *The survival function S_{SS} of the self-similar distribution in radius of $N/S1$ as represented by Eq. (35) (full line), the survival function S_{KR23} of the radius of the Kiang function for $V_p(2,3)$ as represented by Eq. (45) when $\rho = 13$ Mpc, $c = 2.25$ and $\chi^2 = 67.1$ with 100 points (dot-dashed line). The survival function S_{ER23} of the radius of the exponential distribution for $V_p(2,3)$ as represented by Eq. (50) when $\rho = 7$ Mpc and $\chi^2 = 9.27$ with 100 points (dashed line).*

5.2. Exponential distribution of $V_p(2,3)$ in radius

The PDF, $p_{R23}(R;c)$, as a function of the radius corresponding to the exponential distribution as represented by Eq. (38) for $V_p(2,3)$ is:

$$p_{R23}(R;c) = \frac{2\,\mathrm{e}^{-\frac{\pi\,R^2}{\rho^2}} \pi\,R}{\rho^2} \quad , \tag{46}$$

where $0 \leq R < \infty$, $\rho > 0$. The exponential PDF of the radius for $V_p(2,3)$ has the mean:

$$\mu = \frac{\pi^{3/2}}{2\,\rho^2 \left(\frac{\pi}{\rho^2}\right)^{3/2}} \quad , \tag{47}$$

and variance:

$$\sigma^2 = \frac{\rho^2\,(4-\pi)}{4\,\pi} \quad . \tag{48}$$

The DF of the exponential distribution in radius, DF_{ER23}, for $V_p(2,3)$ is:

$$DF_{ER23} = 1 - \mathrm{e}^{-\frac{\pi\,R^2}{\rho^2}} \quad . \tag{49}$$

The survival function S_{ER23} of the radius for $V_p(2,3)$ is:

$$S_{ER23} = \mathrm{e}^{-\frac{\pi R^2}{\rho^2}} \quad . \tag{50}$$

Fig. 4 reports a comparison between the survival function of self-similar voids and the exponential distribution for $V_p(2,3)$.

In this case, the two types of fit in Fig. 4 are satisfactory because we are making a comparison between the observed projected radius of voids and the projected radius of the Voronoi volumes. The smaller χ^2 associated with the exponential distribution can be considered a consequence of the fact that the statistics of the normalized area distribution of the cuts are better described by an exponential distribution than by the Kiang function, see; Table 3.

The final comparison between the four samples of void size statistics as represented in Fig. 4 of von Benda-Beckmann and Müller (2008) and our survival function of the radius of the exponential distribution for $V_p(2,3)$ is reported in Fig. 5.

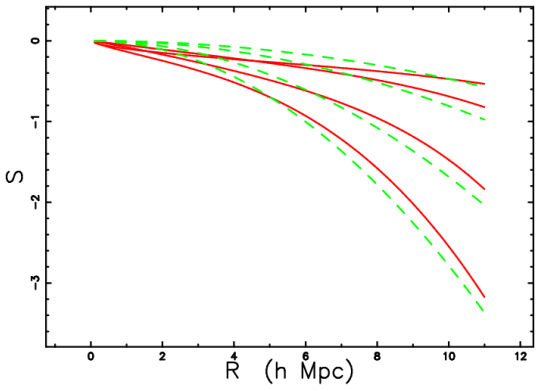

Fig. 5. *The survival function S_{SS} for the self-similar distribution in radius of $N/S1$, $N/S2$, $N/S3$ and $N/S4$, as reported in Fig. 4 of von Benda-Beckmann and Müller (2008) (full lines), as represented by the survival function S_{ER23} of the radius of the exponential distribution for $V_p(2,3)$ as represented by Eq. (50) when $\rho = 7$ Mpc, $\rho = 9$ Mpc, $\rho = 13$ Mpc and $\rho = 17.7$ Mpc (dashed lines).*

6. LARGE-SCALE STRUCTURE

We briefly review the status of the knowledge of the Hubble constant, reference magnitude of the sun, luminosity function of galaxies, Malmquist bias and 3D Poissonian Voronoi diagrams.

6.1. The adopted constants

The first important evaluation of the Hubble constant is through Cepheids (key programs with HST) and type Ia Supernovae; see Sandage et al. (2006), $H_0 = (62.3 \pm 5)$ km s^{-1} Mpc^{-1}. The second important evaluation comes from three years of observations with the Wilkinson Microwave Anisotropy Probe; see Table 2 in Spergel et al. (2007), $H_0 = (73.2 \pm 3.2)k$ km s^{-1} Mpc^{-1}. In what follows, we will take the average value of these two important evaluations: $H_0 = 67.65$ km s^{-1} Mpc^{-1}. The Hubble constant is also reported as $H_0 = 100h$ km s^{-1} Mpc^{-1}, with $h = 1$ when h is not specified; in our case $h = .6765$.

Another quantity that should be fixed in order to continue is the absolute magnitude of the Sun in the b_J filter of the 2dFGRS $\mathcal{M}_\odot = 5.33$; see Colless et al. (2001), Tempel et al. (2009) and Eke et al. (2004).

6.2. Malmquist bias

This bias was originally applied to stars, see Malmquist (1920) and Malmquist (1922), and was then applied to the galaxies by Behr (1951). We now introduce the concept of limiting apparent magnitude and the corresponding completeness in absolute magnitude of the considered catalog as a function of redshift. The observable absolute magnitude as a function of the limiting apparent magnitude, m_L, is:

$$M_L = m_L - 5\log_{10}\left(\frac{c\,z}{H_0}\right) - 25 \quad . \tag{51}$$

The previous formula predicts, from a theoretical point of view, the upper limit on the absolute maximum magnitude that can be observed in a catalog of galaxies characterized by a given limiting magnitude.

The interval covered by the LF of galaxies, ΔM, is defined by:

$$\Delta M = M_{\max} - M_{\min} \quad , \tag{52}$$

where $M_{\max}$ and $M_{\min}$ are the maximum and minimum absolute magnitude of the LF for the considered catalog. The real observable interval in absolute magnitude, ΔM_L, is

$$\Delta M_L = M_L - M_{\min} \quad . \tag{53}$$

We can therefore introduce the range of observable absolute maximum magnitude expressed in percent, $\epsilon(z)$, as:

$$\epsilon_s(z) = \frac{\Delta M_L}{\Delta M} \times 100 \quad . \tag{54}$$

This is a number that represents the completeness of the sample and, given the fact that the limiting magnitude of the 2dFGRS is m_L=19.61, it is possible to conclude that the 2dFGRS is complete for $z \leq 0.0442$. This efficiency, expressed as a percentage, can be considered a version of the Malmquist bias.

6.3. Luminosity function of galaxies

The Schechter function, introduced by Schechter (1976), provides a useful fit for the LF (luminosity function) of galaxies:

$$\Phi(L)dL = (\frac{\Phi^*}{L^*})(\frac{L}{L^*})^{\alpha}\exp\big(-\frac{L}{L^*}\big)dL \quad . \qquad (55)$$

Here, α sets the slope for low values of L, L^* is the characteristic luminosity and Φ^* is the normalization. The equivalent distribution in absolute magnitude is:

$$\Phi(M)dM = (0.4ln10)\Phi^* 10^{0.4(\alpha+1)(M^*-M)} \times \exp\big(-10^{0.4(M^*-M)}\big)dM\,, \quad (56)$$

where M^* is the characteristic magnitude as derived from the data. The parameters of the Schechter function for the 2dFGRS can be found on the first line of Table 3 in Madgwick (2002) and are reported in Table 5.

Table 5. Parameters of the Schechter function for the 2dFGRS.

parameter	2dFGRS
$M^* - 5\log_{10} h$ [mag]	(-19.79 ± 0.04)
α	-1.19 ± 0.01
Φ^* $[h^3\ Mpc^{-3}]$	$((1.59 \pm 0.1)10^{-2})$

We now introduce f, the flux of radiation expressed in units of $L_\odot$ Mpc^{-2}, with $L_\odot$ representing the luminosity of the Sun. The joint distribution in z, redshift and f, see (1.104) in Padmanabhan (1996) or (1.117) in Padmanabhan (2002), is:

$$\frac{dN}{d\Omega dz df} = 4\pi\big(\frac{c_l}{H_0}\big)^5 z^4 \Phi(\frac{z^2}{z^2_{\rm crit}}) \quad , \qquad (57)$$

where $d\Omega$, dz, and df represent the differential of the solid angle, redshift, flux, and c_l represents the speed of light.

This relationship has been derived assuming $z \approx \frac{V}{c_l} \approx \frac{H_0 r}{c_l}$ with r representing the distance of the galaxy in Mpc. The critical value of z, $z_{\rm crit}$, is:

$$z^2_{\rm crit} = \frac{H_0^2 L^*}{4\pi f c_l^2} \quad . \qquad (58)$$

The number of galaxies in z and f as given by Eq. (57) has a maximum at $z = z_{\rm pos-max}$, where:

$$z_{\rm pos-max} = z_{\rm crit}\sqrt{\alpha+2} \quad , \qquad (59)$$

which can be re-expressed as:

$$z_{\rm pos-max} = \frac{\sqrt{2+\alpha}\sqrt{10^{0.4\,M_\odot - 0.4\,M^*}}H_0}{2\sqrt{\pi}\sqrt{f}c_l} \quad . \quad (60)$$

The number of galaxies, $N_S(z, f_{\rm min}, f_{\rm max})$, comprised between the minimum value of flux, $f_{\rm min}$, and the maximum value of flux, $f_{\rm max}$, can be computed from the following integral:

$$N_S(z) = \int_{f_{\rm min}}^{f_{\rm max}} 4\pi\big(\frac{c_l}{H_0}\big)^5 z^4 \Phi(\frac{z^2}{z^2_{\rm crit}}) df \quad . \qquad (61)$$

This integral does not have an analytical solution and, therefore, a numerical integration must be performed. The total number of galaxies in the 2dFGRS is reported in Fig. 6 as well as the theoretical curves obtained by the numerical integration of Eq. (57).

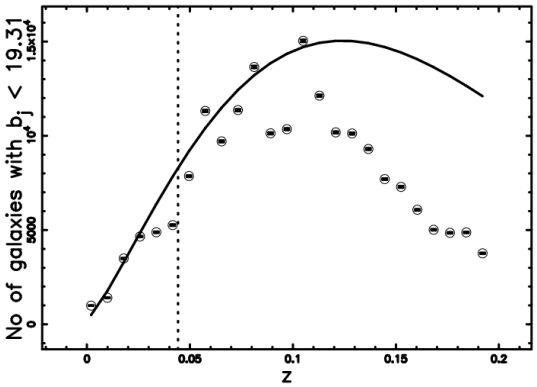

Fig. 6. *The galaxies in the 2dFGRS with* $13.34 \leq bJmag \leq 19.61$ *or 1540* $L_\odot\ Mpc^{-2} \leq f \leq 493844 L_\odot\ Mpc^{-2}$*, are organized as frequencies versus heliocentric redshift (empty stars). The theoretical curve generated by the integral of the Schechter function in flux, Eq. (61), (full line) is drawn. The maximum in the frequencies of observed galaxies is at* $z = 0.108$*. In this plot,* $\mathcal{M}_\odot = 5.33$ *and* $h = 0.67$*. The vertical dotted line represents the boundary between complete and incomplete samples.*

A careful inspection of the previous figure allows to conclude that the theoretical integral fits well the experimental data up to $z = 0.0442$. Beyond this value, the presence of the Malmquist bias decreases the number of observable galaxies and the comparison between the theory and observations cannot be made.

6.4 Voronoi diagrams

Voronoi diagrams represent a useful tool for describing the spatial distribution of galaxies and, as an example, van de Weygaert and Icke (1989) identified the vertexes of irregular Voronoi polyhedrons with Abell clusters. Another example is provided by Zaninetti (1991) where the galaxies were first inserted on the faces of the irregular Voronoi polyhedrons and a power law distribution for the seeds was adopted. Later, the galaxies were still inserted on the faces of the irregular Voronoi polyhedrons but Poissonian seeds were adopted, see Zaninetti (2006, 2008b, 2010a). Adopting the same algorithm developed in Zaninetti (2010a), one slice of the 2dFGRS

with the number of galaxies as a function of z as given by Eq. (61) is simulated; see Fig. 7.

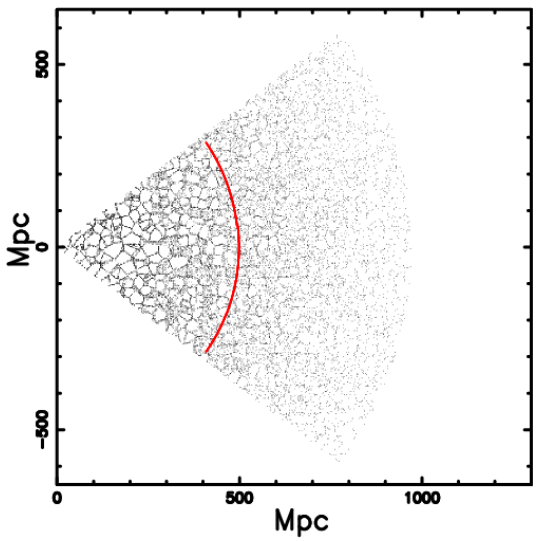

Fig. 7. *A Voronoi slice 75° long and 3° wide. The range of the flux is 2500 $L_\odot$ Mpc^{-2} $\leq f \leq$ 286808$L_\odot$ Mpc^{-2} and the number of galaxies is 19895. The red circle denotes the confusion distance as given by Eq. (64).*

This simulation should be compared with Fig. 1 in von Benda-Beckmann and Müller (2008) and with a 3° slice of the 2dFGRS Image Gallery available at the web site http://msowww.anu.edu.au/2dFGRS/. A little needs to be said about the number of seeds which should be used in order to simulate the observed slices of the 2dFGRS. The average volume of the voids is the side of the box in Mpc divided by the number of seeds. The average diameter of the voids, $D_{\rm Voronoi}$, is:

$$D_{\rm Voronoi} = \left(\frac{\text{side [Mpc]}}{\text{No of seeds}}\right)^{1/3} \quad . \tag{62}$$

The theoretical average diameter $D_{\rm th}$ can be obtained from the average value Eq. (47) of the exponential distribution of $V_p(2,3)$ in radius once the maximum value of ρ which fits the von Benda-Beckmann and Müller (2008) data, see Fig. 5, is adopted:

$$D_{\rm th} = \mu\frac{2}{h} \quad . \tag{63}$$

The equality $D_{\rm Voronoi} = D_{\rm th}$ allows to obtain the number of Poissonian seeds.

A particular attention should be paid to the fact that the astronomical slices are not a plane which intersects a Voronoi network. In order to quantify this effect, we introduce a confusion distance D_c as the distance after which the altitude of the slices becomes equal to the observed average diameter $\overline{D_{\rm obs}}$

$$D_c \tan(\alpha) = \overline{D_{\rm obs}} \quad , \tag{64}$$

where α is the opening angle of the slice and $\overline{D_{\rm obs}}$ is the average diameter of the voids. The case of 2dFGRS $\alpha = 3°$ and therefore $D_c = 498.5$ Mpc when $D_{\rm obs} = 26.12$ Mpc, is illustrated by the red circle in Fig. 7.

7. CONCLUSIONS

The PDFs which are usually used to model the normalized volume distribution of the 3D PVT are gamma type distributions such as the Kiang function, Eq. (3), and the new Ferenc–Neda function, Eq. (14).

Here, in order to make a comparison with the self-similar distribution of voids, we derived the survival distribution of the Kiang function, Eq. (8), and of the Ferenc–Neda function, Eq. (22).

On adopting an astrophysical point of view, the cut $V_p(2,3)$ may model the voids between galaxies as given by astronomical slices of the Millenium catalog. The analysis of the normalized areas of $V_p(2,3)$ is a subject of research rather than a well-established fact and we have fitted them with the Kiang function and the exponential distribution. The χ^2 value indicates that the exponential distribution fits more closely the normalized area distribution of $V_p(2,3)$ than does the Kiang function; see Table 3. This fact follows from the comparison between the self-similar survival function and the exponential and Kiang distributions of the radius; see Fig. 4. Therefore, the one parameter survival function of the radius of the exponential distribution for $V_p(2,3)$, S_{ER23}, as represented by Eq. (50), may model the voids between galaxies as well as the five parameter self-similar survival function.

The observed 2dFGRS slices can be simulated but the behavior of the luminosity function for galaxies and the consequent number of galaxies as a function of the redshift should be carefully analysed.

We are planning, in future projects:

(i) To insert the thickness of the faces of PVT and to model the connected modification of the survival function.

(ii) To apply the technique here developed to the real data sets, Millennium simulation, for example. The 3D nature of the method and detailed density mapping of the voids should be superior to other void identification algorithms as suggested by van de Weygaert and Schaap (2009).

REFERENCES

Aurenhammer, F. and Klein, R.: 2000, In: Handbook of computational geometry ed. Sack, J.-R., Amsterdam: North-Holland.

Barrow, J. D. and Coles, P.: 1990, *Mon. Not. R. Astron. Soc.*, **244**, 188

Behr, A.: 1951, *Astron. Nachr.*, **279**, 97.

Bernardeau, F. and van de Weygaert, R.: 1996, *Mon. Not. R. Astron. Soc.*, **279**, 693.

Chiu, S. N., Weygaert, R. V. D., and Stoyan, D.: 1996, Advances in Applied Probability, **28**, 356.

Coles, P.: 1991, *Nature*, **349**, 288.
Colless, M., Dalton, G., Maddox, S. et al.: 2001, *Mon. Not. R. Astron. Soc.*, **328**, 1039.
Descartes, R.: 1644, Principia Philosophiae, Amsterdam: Ludovicus Elzevirius.
Ebeling, H. and Wiedenmann, G.: 1993, *Phys. Rev. E*, **47**, 704.
Einasto, J., Hütsi, G., Einasto, M. et al.: 2003, *Astron. Astrophys.*, **405**, 425.
Eke, V. R., Frenk, C. S., Baugh, C. M., Cole, S. and Norberg, P.: 2004, *Mon. Not. R. Astron. Soc.*, **355**, 769.
Elyiv, A., Melnyk, O. and Vavilova, I.: 2009, *Mon. Not. R. Astron. Soc.*, **394**, 1409.
Ferenc, J.-S. and Néda, Z.: 2007, *Phys. A*, **385**, 518.
Geller, M. J. and Huchra, J. P.: 1989, *Science*, **246**, 897.
Goldwirth, D. S., da Costa, L. N. and van de Weygaert, R.: 1995, *Mon. Not. R. Astron. Soc.*, **275**, 1185.
Hinde, A. L. and Miles, R.: 1980, *J. Stat. Comput. Simul.*, **10**, 205.
Ikeuchi, S. and Turner, E. L.: 1991, *Mon. Not. R. Astron. Soc.*, **250**, 519.
Jones, D. H., Saunders, W., Colless, M., Read, M. A. and Parker, Q. A. E.: 2004, *Mon. Not. R. Astron. Soc.*, **355**, 747.
Kiang, T.: 1966, *Z. Astrophys.*, **64**, 433.
Madgwick, D. S., Lahav, O., Baldry, I. K. et al.: 2002, *Mon. Not. R. Astron. Soc.*, **333**, 133.
Malmquist, K.: 1920, *Lund Medd. Ser. II*, **22**, 1.
Malmquist, K.: 1922, *Lund Medd. Ser. I*, **100**, 1.
Marinoni, C., Davis, M., Newman, J. A. and Coil, A. L.: 2002, *Astrophys. J.*, **580**, 122.
Melnyk, O. V., Elyiv, A. A. and Vavilova, I. B.: 2006, *Kinematika i Fizika Nebesnykh Tel*, **22**, 283.
Norberg, P., Baugh, C. M., Hawkins, E., Maddox, S. and Madgwick, D. E. A.: 2002, *Mon. Not. R. Astron. Soc.*, **332**, 827.
Okabe, A., Boots, B. and Sugihara, K.: 1992, Spatial Tessellations. Concepts and Applications of Voronoi diagrams, Chichester, NY: Wiley).
Padmanabhan, P.: 2002, Theoretical Astrophysics. Vol. III: Galaxies and Cosmology, Cambridge: Cambridge University Press.
Padmanabhan, T.: 1996, Cosmology and Astrophysics through Problems, Cambridge: Cambridge University Press.
Patiri, S. G., Betancort-Rijo, J. E., Prada, F., Klypin, A. and Gottlöber, S.: 2006, *Mon. Not. R. Astron. Soc.*, **369**, 335.
Pierre, M.: 1990, *Astron. Astrophys.*, **229**, 7.
Press, W. H., Teukolsky, S. A., Vetterling, W. T. and Flannery, B. P.: 1992, Numerical Recipes in FORTRAN. The Art of Scientific Computing, Cambridge: Cambridge University Press.
Sandage, A., Tammann, G. A., Saha, A. et al.: 2006, *Astrophys. J.*, **653**, 843.
Schaap, W. E. and van de Weygaert, R.: 2000, *Astron. Astrophys.*, **363**, L29.
Schechter, P.: 1976, *Astrophys. J.*, **203**, 297.
Spergel, D. N., Bean, R., Doré, O., Nolta, M. R. and Bennett, C. L. E. A.: 2007, *Astrophys. J. Suppl. Series*, **170**, 377.
Subba Rao, M. U. and Szalay, A. S.: 1992, *Astrophys. J.*, **391**, 483.
Tanemura, M.: 2003, *Forma*, **18**, 221.
Tempel, E., Einasto, J., Einasto, M., Saar, E. and Tago, E.: 2009, *Astron. Astrophys.*, **495**, 37.
Tikhonov, A. V.: 2007 *Astronomy Letters*, **33**, 499.
Tinker, J. L., Conroy, C., Norberg, P. et al.: 2008,*Astrophys. J.*, **686**, 53.
van de Weygaert, R.: 1991, *Mon. Not. R. Astron. Soc.*, **249**, 159.
van de Weygaert, R.: 1991, Ph.D. thesis, University of Leiden.
van de Weygaert, R.: 1994, *Astron. Astrophys.*, **283**, 361.
van de Weygaert, R.: 2002, arXiv:astro-ph/0206427
van de Weygaert, R.: 2003, Statistics of Galaxy Clustering - Commentary (Statistical Challenges in Astronomy), 156.
van de Weygaert, R. and Icke, V.: 1989, *Astron. Astrophys.*, **213**, 1.
van de Weygaert, R. and Schaap, W.: 2009, in Lecture Notes in Physics, ed. V. J. Martinez, E. Saar, E. M. Gonzales, and M. J. Pons-Borderia, Berlin: Springer Verlag.
von Benda-Beckmann, A. M. and Müller, V.: 2008, *Mon. Not. R. Astron. Soc.*, **384**, 1189.
Voronoi, G.: 1907, *J. Reine Angew. Math.*, **133**, 97.
Voronoi, G.: 1908, *J. Reine Angew. Math.*, **134**, 198.
Zaninetti, L.: 1991, *Astron. Astrophys.*, **246**, 291.
Zaninetti, L.: 2006, *Chinese J. Astron. Astrophys.*, **6**, 387.
Zaninetti, L.: 2008, *Acta Physica Polonica B*, **39**, 1467.
Zaninetti, L.: 2010, *Revista Mexicana de Astronomia y Astrofisica*, **46**, 115.

ПРАКТИЧНЕ СТАТИСТИКЕ ЗА ПРАЗНИНЕ ИЗМЕЂУ ГАЛАКСИЈА

L. Zaninetti

Dipartimento di Fisica Generale, Via Pietro Giuria 1
10125 Torino, Italy

E–mail: *zaninett@ph.unito.it*

УДК 524.82–17
Оригинални научни рад

Међугалактичке празнине су идентификоване запреминама из Поасон - Вороној формализма. Изведене су две нове функције зависности броја празнина од њиховог радијуса. 2D пројекција Поасон - Вороној мозаика је моделирана Кианговом функцијом и експоненцијалном функцијом. На тај начин су произведене две нове функције броја празнина као алтернатива за функције изведене из "само-сличних" дистрибуција. Симулиране су 2D пројекције из посматрачког каталога 2dF Galaxy Redshift Survey.